Available online at www.sciencedirect.com

ScienceDirect

Energy Procedia 57 (2014) 467 – 476

Energy Procedia

2013 ISES Solar World Congress

Numerical Study of Heat Transfer Losses by Mixed Convection and Surface Thermal Radiation in an Open Cavity Receiver for a Solar Tower System

Armando Piña Ortiz[a], Jesús F. Hinojosa Palafox[a]*, Claudio A. Estrada Gasca[b]

[a]*Departamento de Ingeniería Química y Metalurgía, Universidad de Sonora, Blvd. Luis Encinas y Rosales s/n, Hermosillo, 83000, Sonora, México. Tel. +52 (662) 2592106*

[b]*Instituto de Energías Renovables, UNAM, AP 34, Temixco, 62580, Morelos, Mexico. Tel. +52 (55) 56229744*

Abstract

The thermo solar central tower power plants are complex systems that consist of a heliostats field which provide a high solar concentrated flux to a thermal receiver located in the top of a tower. With this type of technology, a fluid moving in the thermal receiver can be heated up to 800 to 1200 K, so a conventional thermodynamic cycle can be operated to generate electricity. In the city of Hermosillo, in the northern state of Sonora, Mexico, the National Autonomous University of Mexico in agreement with the University of Sonora is developing this type of technology for a plant of 2 MW_t with an array of 80 heliostats (36 m^2 each one) and a tower of 32 m height. Therefore, an appropriated thermal receiver has to be designed. Considering above, in this work the numerical results of heat transfer losses by mixed convection and surface thermal radiation in an open cavity receiver considering variable fluid properties are presented. Numerical calculations were performed in a cavity of 1 m width, 2 m height and 2 m depth, considering (a) only natural convection and (b) mixed convection, both with surface thermal radiation. The temperature difference between the hot wall and the bulk fluid (ΔT) was 600 K. The k_t-ε_t standard turbulence model was solved for the turbulent convection and for the surface thermal radiation the discrete ordinate method was applied. The simulations were conducted in steady state and the fluid properties were considered as a function of temperature. The software of computational fluid dynamics FLUENT 6.3 was used. The velocity, temperature fields and heat transfer coefficients were obtained. The total heat transfer losses increases 37.5% when the mixed convection is considered.

Selection and/or peer-review under responsibility of ISES.

Keywords: numerical, heat transfer, open cavity

* Corresponding author. Tel.: +52(662)2592106

E-mail address: fhinojosa@iq.uson.mx

Selection and/or peer-review under responsibility of ISES.

doi:10.1016/j.egypro.2014.10.200

1. Introduction

Nowadays energy is essential for the sustaining of society since it is used for almost all human activities like transportation, illumination, heating, cooling, education, food and industrial production, etc. Current economic systems are based on oil technologies and at least 90% of the CO_2 emission amount result from fossil fuels burning for power generation and transport sector [1]. Furthermore, petroleum (and natural gas) price is expected to step up in the next two decades, from $125/barrel in 2011 to over $215/barrel in 2035 [1]. One of the options, in the renewable energies spectrum to tackle these problems, is the concentrating solar thermal systems that consists, basically, in an array of mirrors which pick up sun light and concentrates unto a receiver. The central receiver system (CRS) concept could not only provide cheaper electricity (compared with other CSP options) but also a better performance. Some of the advantages of the CRS are: readily integration in fossil plants for hybrid operation, higher temperatures (up to 1000 °C) and thereby higher efficiency, etc [2]. In a CRS, the solar receiver is the heat exchanger where the solar radiation is absorbed and transformed into thermal energy useful in power conversion systems [3]. The heat losses in the open cavity receiver for the CRS are mainly by convection and thermal radiation, it is therefore very important to fully understand the basic behavior of these heat transfer mechanisms [4]. The studies reported in the literature of cavity receivers for solar central tower systems are briefly described below. In the late seventies Hildebrandt and Vant-Hull [5] discussed the feasibility of the CRS concept and since then it has made substantial progress in the field. Zoschak et al. [6] performed the design and testing of a cavity-type, steam-generating, central receiver for a solar thermal power plant where they confirmed the receiver design for an operational north field cavity central receiver power plant. Clausing [7] conducted an analysis using an analytical model of heat losses in cavity receivers. Two receiver sizes were considered: 1 MW and 38 MW. The first has an opening of 1 m^2, T_∞ =20°C and a heat exchanger temperature of 725°C, while the second has an aperture of 40 m^2, T_∞=20°C and a heat exchanger temperature of 725°C. The model indicates that the influence of wind on heat loss, for normal operating conditions (8 m/s or less) is minimal. The heat losses for receivers of 1 MW and 38 MW, are 6.8% and 8.9% respectively. Clausing [8] presented an analytical model of convection losses for a solar cavity receiver, where are compared the analytical predictions and the experimental results of a cubic cavity with 0.6 m on a side, considering a temperature range of 120-138 °C. In this study it is mentioned that the cavity solar receivers have higher thermal efficiencies that external receivers due to reduced heat losses. If the receiver contains a large amount of inactive area in the hot wall, may experience high convective heat losses. McMordie [9] conducted experimental tests to resolve the uncertainties involved in predicting the convective heat losses. The receiver was designed to absorb 5 MW of solar energy and to use molten salt as heat transfer fluid. The receiver absorption area was 5.6 x 3.5 m, with a height of 3.5 m, while the opening of the cavity has dimensions of 2.7 x 2.7 m. Heat losses by convection were determined by calculating analytically the radiation and conduction losses and subtracting the sum of these two to the total losses. On average convective heat losses were 1.43 % of the total heat supplied. Kribus et al. [10] performed an experiment to demonstrate that splitting the opening of the thermal receiver in separate stages according to the distribution of irradiation can significantly reduce the heat losses by convection. The high temperature receiver stage is the annular pressurized receiver direct irradiation. The low temperature stage is implemented as a partial ring of intermediate temperature cavity tubular receivers (preheater) surrounding the central high temperature stage. Following the initial concentration of the one part of the heliostat field, the solar radiation enters the receiver via compound parabolic concentrators. The outlet air temperatures were of 1000 °C, with the low temperature stage supplying up to 750 °C. The output power became up to 55 kWt. Hasuike et al. [11] conducted a study that took into account systems using molten salt as heat transfer fluid. They considered a cavity receiver for a beam-down solar concentration system.

The optimal characteristics of the receiver design were predicted with a developed numerical simulation program. Radiation to heat conversion efficiency is calculated from input solar power and heat transferred to molten salt, and it is about 90%. Kim et al. [12] presented experimental data that describe the convective heat transfer in a cavity receiver. The cavity receiver had a cross section of 2 x 2 m and the following conditions were considered: 4 different types of cavities, three surface temperatures of the receiver (300, 400 and 500 °C), wind speed between 2 and 8 m/s and four different tilt angles. It was observed that convection losses are not related with the opening position and the distance between the aperture and the heater. Wang et al. [13] carried out a numerical simulation using the Monte Carlo method to predict the heat flux distribution in the cavity receiver, which consists of six flat sides and ceiling and floor, with an opening of 2 x 2 m on the front face. When considering radiative exchange between the walls, was determined that 49.10% of the total incident energy was absorbed by the central panels, 47.02% by side panels and a 3.88% overflow through the opening. The peak heat flow was 1196.41 kW/m^2 at the center of the absorber wall. Yao et al. [14] carried out the modeling and simulation of the pioneer thermal central receiver plant of 1 MW in China. The model of the entire plant was established with TRNSYS. It was found that the emission and convection losses make up the majority of the thermal losses from the receiver. The simulation results agree well with published data of the heliostat field of PS10 in Spain. Li et al. [15] developed a steady state model of a molten salt cavity receiver (60% $NaNO_3$ and 40% KNO_3) of 100 kW_t. In the design process the following factors were analyzed: receiving area, heat losses (convective, emissive, reflective and conductive), number of tubes in the receiver panel, tube diameter and temperature of the receiving surface. The receiver surface ranged from 0.1 m^2 to 1 m^2. By increasing the receiving area the surface temperature decreased and increased the convective, reflective and conductive heat losses. Of the total heat losses, a 25.37% were due to convection when the receiving area was 0.1 m^2 and was 56.04% for a receiving area of 1 m^2. Fang et al. [16] conducted a combined calculation method to evaluate the thermal performance of a solar cavity receiver with an irregular octahedral geometry and dimensions of 4 x 4 m for the opening, and 8.25 x 3 m for the walls. The method couples the Monte-Carlo method, the correlations of heat transfer for boiling flows and calculations of the air flow field. The method can estimate the heat flux distribution on the surfaces of the cavity, the wall temperature of the hot tubes, and the heat losses of the solar receiver with an iterative solution. The higher intensity of radiative flux occurs in the roof of the cavity, obtaining a maximum temperature of 640 °C. The air speed reaches a maximum value when the wind is coming from one side of the receiver. Heat losses in the cavity receiver reaches a maximum value for wind parallel to the opening of the cavity. The heat loss for a speed of 3 m/s is 11% of total solar energy in the opening, for 6 m/s is 14%, and for 9 m/s is about 17%. The literature review indicates that there are not reported three-dimensional numerical studies in an open cavity receiver considering variable fluid properties and mixed convection coupled with surface thermal radiation. Considering the above, this paper presents a detailed numerical analysis of the heat transfer by natural and mixed convection with surface thermal radiation in an open cavity receiver with turbulent flow. The numerical results were obtained considering a fixed temperature of 900 K for the hot wall, 300 K for the rest of the surfaces of the cavity and an emissivity value of 0.95 for all surfaces. The velocity and temperature fields and heat transfer coefficients are presented and discussed.

2. Physical model

The study of the heat transfer by convection and surface thermal radiation was carried out in a cavity of 1m width, 2 m height and 2 m depth as is shown in Figure 1. The left vertical wall was fixed at a T_h temperature meanwhile the rest of the cavity walls are considered as adiabatic.

The thermal fluid is air and it is not involved in radiative heat transfer, therefore radiative exchange is between the walls of the cavity. The numerical results were obtained considering an emissivity of 0.95 for all the surfaces. The fluid flow is assumed as turbulent.

3. Mathematical model

The governing equations (mass conservation, momentum and energy), in time averaged tensor notation, for the steady state, are as follow:

Continuity:

$$\frac{\partial \bar{u}_i}{\partial x_i} = 0 \tag{1}$$

Momentum:

$$\rho \bar{u_j} \frac{\partial \bar{u_i}}{\partial x_i} = \frac{\partial \bar{P}}{\partial x_i} + \frac{\partial}{\partial x_j}\left[\mu \frac{\partial \bar{u_i}}{\partial x_j} - \rho \overline{u_i' u_j'}\right] + \rho g_i \tag{2}$$

Energy:

$$\rho \bar{u_j} \frac{\partial \bar{T}}{\partial x_j} = \frac{1}{C_p} \frac{\partial}{\partial x_j}\left[k \frac{\partial \bar{T}}{\partial x_j} - \rho C_p \overline{T' u_j'}\right] \tag{3}$$

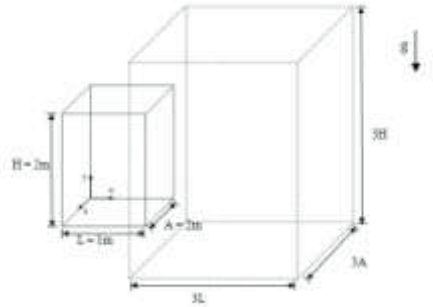

Figure 1. Scheme of the cavity with extended domain.

where x_i and x_j are the Cartesian coordinates of the system (i= *x*, *y* , *z* and j=*x*, *y*, *z*), $\bar{u}$ is the mean velocity, $\bar{P}$ is the mean dynamic pressure, $\bar{T}$ is the mean temperature, *g* is the gravitational acceleration; *k*, ρ, μ, Cp are the thermal conductivity, the density, the viscosity and the specific heat at constant pressure, respectively. The turbulent kinetic energy (k_t) and the dissipation of the turbulent kinetic energy (ε_t) are obtained from their transport equations by using the k_t - ε_t model developed by Ince and Launder [17]:

Turbulent kinetic energy (k_t):

$$\rho \bar{u_j} \frac{\partial \bar{k_t}}{\partial x_j} = \frac{\partial}{\partial x_j}\left[\left(\mu + \frac{\mu_t}{\sigma_{k_t}}\right)\frac{\partial \bar{k_t}}{\partial x_j}\right] + P_{k_t} + G_{k_t} + \rho\varepsilon_t \tag{4}$$

Dissipation of the turbulent kinetic energy (ε_t):

$$\rho u_j \frac{\partial \varepsilon_t}{\partial x_j} = \frac{\partial}{\partial x_j}\left[\left(\mu + \frac{\mu_t}{\sigma_{\varepsilon_t}}\right)\frac{\partial \bar{\varepsilon_t}}{\partial x_j}\right] + C_{1\varepsilon_t}\frac{\varepsilon_t}{k}\left[P_{k_t} + C_{3\varepsilon_t} G_{k_t}\right] - C_{2\varepsilon_t}\rho\frac{\varepsilon_t^2}{k_t} \tag{5}$$

In the above equations, P_{k_t} represents the generation of the turbulent kinetic energy caused by velocity gradients and G_{k_t} is the generation of turbulent kinetic energy due to the buoyancy force. The terms $C_{1\varepsilon_t}$, $C_{2\varepsilon_t}$ and $C_{3\varepsilon_t}$ are coefficients; whereas σ_{k_t} and σ_{ε_t} are the turbulent Prandtl number for the equations of k_t and ε_t, respectively.

The no slip assumption is applied as hydrodynamic boundary condition for all the surfaces of the cavity. The wall opposite to the aperture has a fixed temperature (T_h) whilst the rest of the surfaces are considered as adiabatic. The values of turbulent kinetic energy and dissipation of turbulent kinetic energy are zero on the walls of the cavity, since for the near wall treatment several wall functions were tested showing no appreciable effects. For the extended domain von Neumann conditions are assumed for temperature, velocity and turbulent variables, except in the case of mixed convection where one side of the extended domain is fixed a value of velocity. The radiative energy transfer in an anisotropic medium which absorbs, emits and scatters radiation, is described mathematically by the radiative transfer equation:

$$\frac{dI_\eta}{ds} = k_\eta I_{b_\eta} - \beta_\eta I_\eta + \frac{\sigma_{s\eta}}{4\pi}\int_{4\pi} I_\eta(\hat{s}_i)\Phi_\eta(\hat{s}_i,\hat{s})d\Omega_i \tag{6}$$

where I_η is the intensity of radiation, $\hat{s}$ is the geometric path length, $\hat{s}_i$ is the unit vector in a given direction, I_{b_η} is the blackbody intensity, k_η is the absorptivity, β_η is the coefficient of extinction, $\sigma_{s\eta}$ is the scattering coefficient and Ω_i is the solid angle. However, because the air is considered as non-participating media, the Eq. (6) becomes:

$$\frac{dI}{dS} = 0 \tag{7}$$

The Eq. (7) indicates that the intensity of radiation is constant along a given path length and that the radiation heat transfer occurs through radiative exchange among the walls of the cavity. With the purpose of generalize the results, the non-dimensional Rayleigh and Reynolds numbers, were defined as:

$$Ra = \frac{g\beta(T_h - T_\infty)L^3}{\alpha\upsilon} \tag{8}$$

$$Re = \frac{UH}{\upsilon} \tag{9}$$

where υ is the kinematic viscosity, β is the thermal expansion coefficient, T_h and T_∞ is the temperatures of the isothermal wall and bulk fluid temperature, respectively. The convective Nusselt number is defined as the ratio between the heat flux at the hot wall in the presence of natural convection and the heat flux due to conduction only. In mathematical form:

$$Nu_c = \frac{q_{conv}}{q_{cond}} = \frac{q_{conv}}{k_{average}(T_H - T_\infty)/H} \tag{10}$$

where $k_{average}$ was computed at the average temperature between the isothermal wall and the ambient air. The average convective Nusselt number in the cavity ($\overline{Nu_c}$) was obtained by integrating the local Nusselt number over the area of the isothermal wall. The radiative Nusselt number is defined as the ratio between the radiative heat flux at the hot wall and the heat flux due to conduction only, then:

$$Nu_r = \frac{q_{rad}}{q_{cond}} = \frac{q_r(0,0<\mathrm{Y}\le \mathrm{H},0<\mathrm{Z}\le \mathrm{A})}{k_{average}(T_H - T_\infty)/H} \tag{11}$$

The average radiative Nusselt number ($\overline{Nu_r}$) was obtained by integrating the radiative Nusselt numbers over the isothermal wall. The total average Nusselt number ($\overline{Nu_t}$) was calculated by summing the average convective Nusselt number and the average radiative Nusselt number.

4. Numerical method

The numerical results were obtained using the CFD software Fluent 6.3, which is based on the finite volume method in order to solve the governing equations of the fluid dynamics. For the coupling of the momentum and continuity equations the SIMPLE algorithm was used. The convective terms were

discretized applying the MUSCL scheme [18]. The radiative heat transfer model was solved with the discrete ordinate method; in this method the radiative model is solved for a series of n different directions ($\hat{s}_i$) assuming that the intensity remains constant within the control volume and the integrals are approximated using a Gaussian quadrature all over the solid angle. A uniform mesh with greater node density on the x direction was used. The averaged Nusselt number on the isothermal wall was independent of the mesh size, when the grid size was 60x70x70 (2.94 $x10^5$ nodes). The convergence was achieved when the weighted residue of each of the governing equations was 10^{-3}. Due to the difficulty of the establishment of the boundary conditions in the aperture area, a extended domain was annexed with a dimension of 3 m in the *x* direction and 6 m in the *y* and *z* directions which can be seen as the dotted lines in Figure 1. The mesh size for the extended domain was fixed at 10x70x70 ($4.9x10^4$ nodes). In this work the air property variations with the temperature are modeled using seventh grade polynomials, whose coefficients are presented in Table 1.

5. Results

The study of the open cavity receiver was performed considering a temperature value of 900 K on the isothermal wall with a corresponding Rayleigh number of $1.82x10^{12}$. The extended domain temperature was fixed at 300 K. For the case of mixed convection in the right vertical wall of the extended domain (at z=2A) was set a velocity value of 5 m/s, equivalent to a Reynolds number of $6.25x10^5$.

5.1 Velocity magnitude fields

Figure 2 shows the velocity magnitude for a plane at z = 1 m (central vertical plane) of the cavity for the case a) natural convection only (NC) and b) mixed convection (MC). It can be observed that for the NC case the fluid enters at the bottom of the cavity with a velocity of 0.4 m/s moves towards the isothermal wall reaching a maximum value of 1.0 m/s and finally leaves the cavity slowing down to 0.9 m/s. Whilst, for the MC case the fluid enters with a velocity of 3 m/s and slows down to a value of 2 m/s in the isothermal wall and the superior surface of the cavity. It can be seen the lowest value of velocity for the MC case of 0.5 m/s whilst for the NC case this value decrease to 0.1 m/s. In Figure 3 the velocity magnitude for the aperture area of the cavity shows that for the NC case the fluid enters symmetrically at a value of 0.4 m/s in the lower and leaves the cavity with a velocity of 1.6 m/s. Whilst, for the MC case the fluid enters with a maximum value of 2.8 m/s at the 1.3 m of the z coordinate and this value decreases till 1.2 m/s at the left side of the aperture; in this case the symmetry cannot be seen due to the air stream.

5.2 Temperature fields

Figure 4 shows the temperature field at a plane at z= 1m, for both cases (NC and MC) a mayor proportion of the cavity has temperature value of 350 K and the thermal boundary layer of approximately 0.03 m in the isothermal wall where the temperature moves from 850 K until 350 K. Also, in the inferior surface of the cavity it can be seen a thermal boundary layer smaller than the one from the isothermal wall. In the NC case the superior part shows a uniform thermal boundary layer, whilst for the MC case this uniformity is broken and the superior surface shows mayor stratification where are temperature values ranging from 650 K to 400 K.

5.3 Heat transfer analysis

In Figure 5 the contours of total heat flux in the isothermal wall (x=0) show that for the NC case the maximum value in the center area of the surface is 32 kW/m^2 and decreases to 20 kW/m^2 at the perimeter of the surface. Whilst for the MC case the maximum value of total heat flux is 35 kW/m^2 in the lower central section and decreases to 25 kW/m^2 at the perimeter. Again, the symmetry in the MC is case is broken due to the air stream as it can be seen in the Figure 2. In Table 3 are presented the heat transfer losses by radiation and convection. The radiative losses of the isothermal wall are 106.1 kW/m^2 for the mixed convection case and 101.6 kW/m^2 for the natural convection case. The convective losses are 57%

bigger for the mixed convection case compared with the natural convection case due to the presence of the air stream which acts as a withdrawing heat removal source, whereas the total losses are 11% bigger for the mixed convection cases compared with the natural convection case. In Table 4 are presented the averaged Nusselt numbers (radiative, convective and total) for the isothermal wall as well as the heat transfer coefficients (radiative, convective and total). As it can be seen the radiative contribution is 87 % of the total for the natural convection case whilst for the mixed convection case this mechanism contributes with the 81.5 % of the total. The convective heat transfer contributes with 13 % and 18.5 % for the NC case and MC case, respectively. The total Nusselt number is 11% bigger for the mixed convection case.

Table 1. Coefficients of the polynomial adjustment of thermophysical properties.

Coefficients	ρ (kg/m^3)	C_p (J/kg K)	k (W/m K)	μ (kg/m s)
a	5.467574143	1203.42803	0.061296206	-6.29158×10^{-6}
b	-0.03644233	-2.05649456	-0.000645759	1.6655×10^{-7}
c	0.000134708	0.008703624	3.71597×10^{-6}	-5.95923×10^{-10}
d	-3.02101×10^{-7}	-2.03614×10^{-5}	-1.02557×10^{-8}	1.76719×10^{-12}
e	4.21124×10^{-10}	2.98834×10^{-8}	1.65126×10^{-11}	-3.28629×10^{-15}
f	-3.56688×10^{-13}	-2.61465×10^{-11}	-1.56764×10^{-14}	3.60618×10^{-18}
g	1.6805×10^{-16}	1.22738×10^{-14}	8.12384×10^{-18}	-2.12792×10^{-21}
h	-3.37707×10^{-20}	-2.35884×10^{-18}	-1.76913×10^{-21}	5.18944×10^{-25}

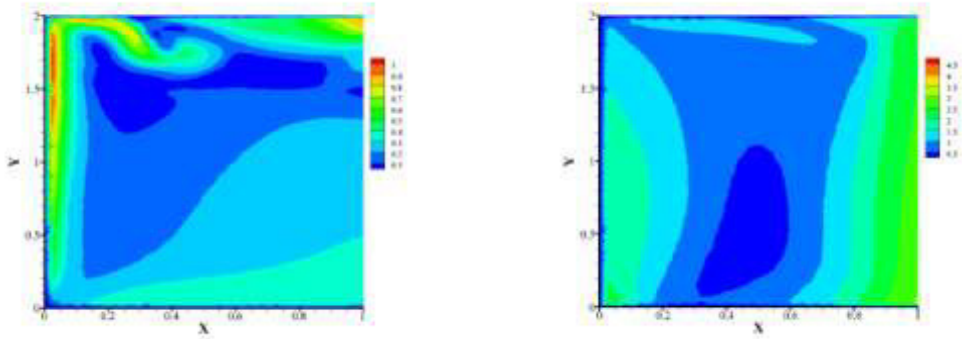

Figure 2. Velocity magnitude at Z= 1m for pure natural convection (left) and b) Mixed convection (right).

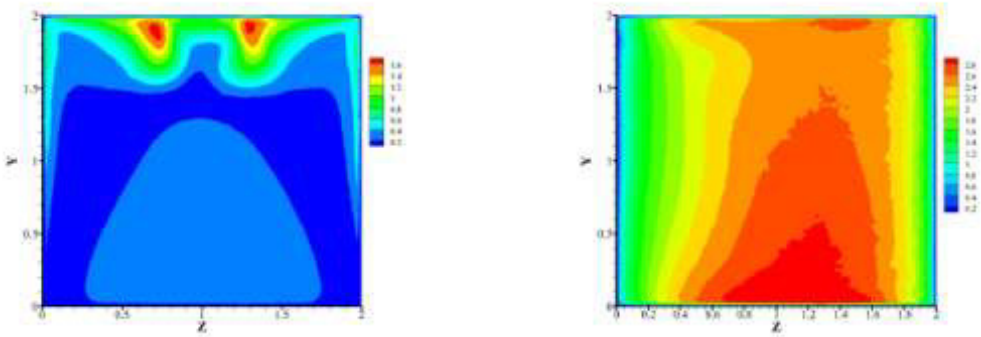

Figure 3. Velocity magnitude at X=1m. Pure natural convection (left) and b) Mixed convection (right).

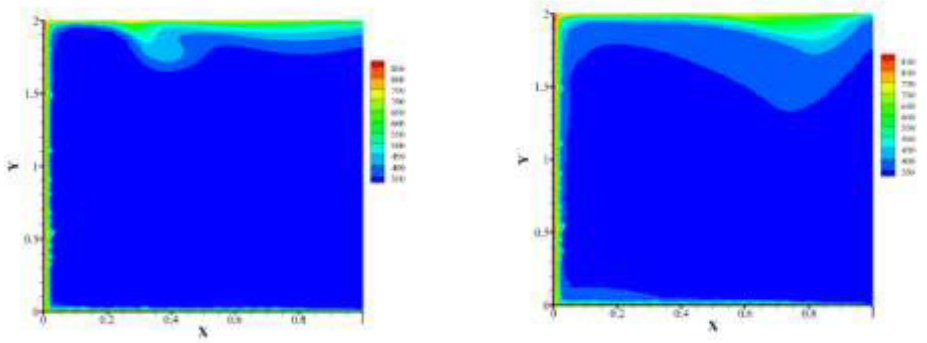

Figure 4. Temperature fields (K) at Z=1 m, for pure natural convection (left) and b) Mixed convection (right).

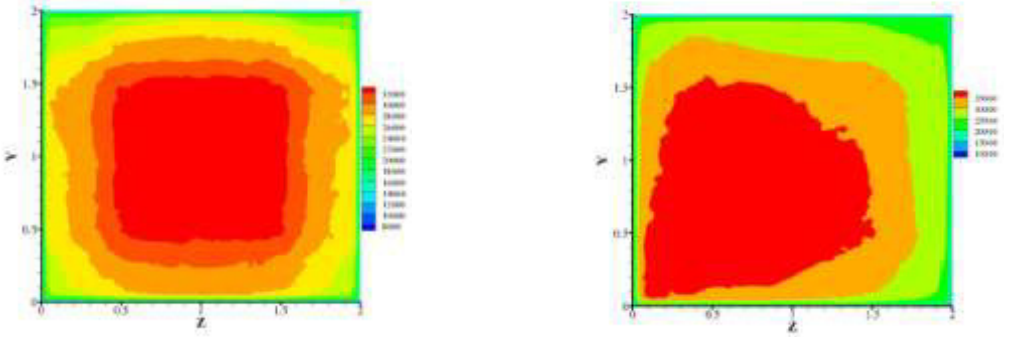

Figure 5. Total heat flux contours (W/m^2) at isothermal wall (X=0), for pure natural convection (left) and b) Mixed convection (right).

Table 3. Heat transfer losses.

Case	Radiative Losses (kW/m^2)	Convective Losses (kW/m^2)	Total Losses (kW/m^2)
Natural convection	101.6	15.2	116.8
Mixed convection	106.1	23.9	130.0

Table 4. Heat transfer coefficients.

Case	h_c (W/m^2·K)	Nu_r	Nu_c	Nu_t
Natural convection	25.3	7221.0	1080.3	8301.4
Mixed convection	39.8	7540.9	1698.6	9239.5

6. Conclusions

From the results we can conclude the following:

- When pure natural convection is considered at the aperture of the cavity symmetry is appreciated whilst this behavior is broken due to the presence of an air stream.
- At the interior of the cavity for pure natural convection the maximum values of velocity of the fluid are at the boundary layer adjacent to the isothermal wall whilst for the mixed convection case the fluid enters with a high value and it slows down while it approaches to the isothermal wall.
- In both cases the fluid temperature in the cavity interior are almost uniform at 350 K, but the mixed convection case shows a larger temperature stratification in the proximity of the top wall.
- The total heat fluxes in the isothermal wall are higher for the mixed convection case.
- In both cases the radiative heat transfer mechanism is the mayor contributor to overall heat transfer with values of 87 % and 81.5 % for the natural and mixed convection cases, respectively.
- The presence of an air stream of 5 m/s entering parallel to the aperture causes an increase of 11 % in the total heat transfer losses comparing with a case in which only natural convection is considered.

Nomenclature

A	Cavity depth, m	u´	Instant fluctuation of x-velocity direction, m/s
C_p	Specific heat, J / kg K	U	Inlet velocity, m/s
g	Gravity, m/s^2	$\bar{u}_i$	Time averaged velocity on i direction, m/s
G$_k$	Generation of turbulent energy due to the buoyancy forces	X, Y, Z	System coordinate (i= x, y, z)
h_c	Convective heat transfer coefficient, W/m^2 K	Greek symbols	
h_r	Radiative heat transfer coefficient, W/m^2 K	α	Thermal diffusivity, m^2/s
h_t	Total heat transfer coefficient, W/m^2 K	β	Thermal expansion coefficient, 1/K
H	Cavity height, m	β_η	Extinction coefficient, nondimensional
I_η	Intensity of radiation, W/m^2	ε	Emissivity, nondmensional
$I_{b\eta}$	Blackbody intensity, W/m^2	εt	Turbulent kinetic energy dissipation, m^2/s^3
k	Thermal conductivity, W/m K	Ω_i	Solid angle, sr
k_t	Turbulent kinetic energy, m^2/s^2	υ	Kinematic viscosity, m^2/K
k_η	Absorptivity, nondimensional	μ	Viscosity, kg /m s
L	Cavity width, m	μ_t	Turbulent viscosity, kg/m s
N u$_c$	Convective Nusselt number, nondimensional	ρ	Density, kg/m^3
N u$_r$	Radiative Nusselt number, nondimensional	σ_T	Turbulent Prandtl number for energy equation, nondimensional
N u$_t$	Total Nusselt number, nondimension	υ_{k_t}	Turbulent Prandtl number for k_t equation, nondimensional
P	Pressure, Pa	υ_{ε_t}	Turbulent Prandtl number for ε_t equation, nondimensional
P_k	Generation of turbulent kinetic energy due to velocity gradients	$\sigma_{s\eta}$	Scattering coefficient, nondimensional
R	Rayleigh number, nondimensional	Subscripts	

a			
Re	Reynolds number, nondimensional	c	Convective
$\hat{s}$	Geometric path length, m	r	Radiative
$\hat{s}_1$	Unit vector, nondimensional	*i, j*	*i*th and *j*th elements
T	Mean temperature, K	t	Total
T_h	Temperature of isothermall wall, K	∞	Ambient
T_∞	Temperature of bulk fluid, K		

References

[1] World Energy Outlook. Executive summary; 2012, www.worldenergyout look.org/.

[2] Renewable energy technologies: cost analysis series. Volume 1: power sector issue 2/5, Concentrating solar power. IRENA, June; 2012.

[3] Behar O, Khellaf A, Mohammedi K, A review of studies on central receiver solar thermal power plants, Renewable and Sustainable Energy Reviews 2000; 23: 12-39.

[4] Montiel G M, Hinojosa J P, Estrada A C, Numerical study of heat transfer by natural convection and surface thermal radiation in an open cavity receiver. Solar Energy 2012;86:1118–28.

[5] Hildebrandt A. F, Vant-Hull L. L,Power with Heliostats, Science 1977; 197-4309.

[6] Zoschak R J, Wu S F, Gorman D N,Design and Testing of a Cavity-Type, Steam-Generating, Central Receiver for a Solar Thermal Power Plant, J. Eng. Power 1980; 102-2: 486-494.

[7] Clausing, A. M, An Analysis of Convective Losses From Cavity Solar Central Receivers, Sol. Energy 1981;**27**~4: 295–300.

[8] Clausing, A. M, Convection Losses From Cavity Solar Receivers- Comparisons Between Analytical Predictions and Experimental Results;J. Sol. Energy Eng.1983;**105**:29–33.

[9] McMordie, R. K. Convection heat loss from a cavity receiver. J. Sol. Energy Eng. 1984;106: 98.

[10] Kribus, A., Doron, P., Rubin, R., Karni, J., Reuven, R., Duchan, S., Taragan, E. A multistage solar receiver: the route to high temperature. Solar Energy. 1999;67: 3.

[11] Hasuike, H., Yoshizawa, Y., Suzuki, A., Tamaura, Y. Study on design of molten salt solar receivers for beam-down solar concentrators. Solar Energy. 2006;80: 1255.

[12] Kim, J. K., Yoon, H. K., Kang, Y. H. Experimental study on heat loss from cavity receiver for solar power tower. Proceedings of ISES Solar World Congress 2007: Solar Energy and Human Settlement. 2007;5:1719.

[13] Wang, Y., Dong, X., Wei, J., Jin, H. Numerical simulation of the heat flux distribution in a solar cavity receiver. Frontiers of Energy and Power Engineering in China. 2009;4:571.

[14] Yao, Z., Wang, Z., Lu, Z., Wei, X. Modeling and simulation of the pioneer 1 MW solar thermal central receiver system in China. Renewable Energy. 2009;34:2437.

[15] Li, X., Kong, W., Wang, Z., Chang, Ch., Bai, F. Thermal model and thermodynamic performance of molten salt cavity receiver. Renewable Energy. 2010;35:981.

[16] Fang, J. B., Wei, J. J., Dong, X. W., Wang, Y. S. Thermal performance simulation of a solar cavity receiver under windy conditions. Solar Energy. 2011;85:126.

[17] Ince N.Z, Launder, B.E, On the Computation of Buoyancy Driven Turbulent Flows in Rectangular Enclosures, International Journal of Heat and Fluid Flow, 1989;10: 110-117

[18] Van Leer B, Toward the Ultimate Conservative Difference Scheme. IV. A Second Order Sequel to Godunov's Method. Journal of Computational Physics, 1979; 32:101-136